

# Thermal evolution of defects in as-grown and electron-irradiated ZnO studied by positron annihilation

Z. Q. Chen\* and S. J. Wang

*Hubei Nuclear Solid Physics Key Laboratory, Department of Physics, Wuhan University, Wuhan 430072, People's Republic of China*

M. Maekawa, A. Kawasuso, and H. Naramoto

*Advanced Science Research Center, Japan Atomic Energy Agency, 1233 Watanuki, Takasaki, Gunma 370-1292, Japan*

X. L. Yuan and T. Sekiguchi

*Nanomaterials Laboratory, National Institute for Materials Science, 1-2-1 Sengen, Tsukuba, Ibaraki 305-0047, Japan*

(Received 31 January 2007; published 13 June 2007)

Vacancy-type defects in as-grown ZnO single crystals have been identified using positron annihilation spectroscopy. The grown-in defects are supposed to be zinc vacancy ( $V_{\text{Zn}}$ )-related defects, and can be easily removed by annealing above 600 °C.  $V_{\text{Zn}}$ -related defects are also introduced in ZnO when subjected to 3 MeV electron irradiation with a dose of  $5.5 \times 10^{18} \text{ cm}^{-2}$ . Most of these irradiation-induced  $V_{\text{Zn}}$  are annealed at temperatures below 200 °C through recombination with the close interstitials. However, after annealing at around 400 °C, secondary defects are generated. A detailed analysis of the Doppler broadening measurements indicates that the irradiation introduced defects and the annealing induced secondary defects belong to different species. It is also found that positron trapping by these two defects has different temperature dependences. The probable candidates for the secondary defects are tentatively discussed in combination with Raman scattering studies. After annealing at 700 °C, all the vacancy defects are annealed out. Cathodoluminescence measurements show that  $V_{\text{Zn}}$  is not related to the visible emission at 2.3 eV in ZnO, but would rather act as nonradiative recombination centers.

DOI: [10.1103/PhysRevB.75.245206](https://doi.org/10.1103/PhysRevB.75.245206)

PACS number(s): 61.72.Ji, 78.70.Bj, 71.55.Gs

## I. INTRODUCTION

ZnO is a II-VI compound semiconductor with wide band gap of 3.4 eV and large exciton binding energy of 60 meV. These features enable its potential application in short wavelength light emitting devices. Due to the successful fabrication of large area ZnO single crystals,<sup>1</sup> there is a growing interest in the investigation of this materials in recent years.<sup>2,3</sup> Among these investigations, study of defects is one of the most important subjects because of the strong influence of these defects on the electrical and optical properties. Due to deviation from the chemical stoichiometry, various defects are introduced inevitably after crystal growth. It is known that the native defects, such as zinc interstitial ( $\text{Zn}_i$ ) and oxygen vacancy ( $V_{\text{O}}$ ), might be the reason for the intrinsic  $n$ -type conduction in undoped ZnO.<sup>4,5</sup> These defects will also compensate acceptors and cause difficulty in producing  $p$ -type ZnO.<sup>6</sup> On the other hand, defects may also act as nonradiative recombination centers and degrade the light emission efficiency.

There have been several theoretical investigations on native defects in ZnO,<sup>6-9</sup> which calculated the formation energy and ionization level of various defects. A variety of experiment methods have also been used to characterize the defects in ZnO, such as electron paramagnetic resonance (EPR), photoluminescence, cathodoluminescence (CL), and deep level transient spectroscopy (DLTS). These methods provided detailed information about defects from different aspects. However, direct discrimination of defects in ZnO is always a difficult problem because of the limitation of these methods. Until now, there are still some fundamental prob-

lems in which no clear consensus seems to exist. For example, the EPR signal of  $g=1.96$  was attributed to oxygen vacancy,<sup>10</sup> but some others argued that the oxygen vacancy signal was at  $g=1.99$ .<sup>11</sup> The green luminescence at about 2.4 eV was correlated with oxygen vacancy by many researchers,<sup>12-15</sup> but it was also attributed to other defects such as  $V_{\text{Zn}}$ ,<sup>16,17</sup>  $\text{Zn}_i$ ,<sup>18,19</sup>  $\text{O}_{\text{Zn}}$ ,<sup>20,21</sup> and even Cu impurities.<sup>22</sup> DLTS revealed a major defect level L2 at  $E_c - 0.3 \text{ eV}$  in the as-grown ZnO, but the assignment of this level is also rather difficult.<sup>23</sup>

Positron annihilation spectroscopy (PAS) has been proven to be a powerful tool for the study of vacancy-type defects in semiconductors.<sup>24</sup> When positrons are emitted into materials, they will first lose their energy (thermalization) in a few picoseconds, then diffuse inside the lattice. If there are vacancy-type defects within the range of positron diffusion length, positron will be trapped by these vacancies. Due to the reduced electron density and lower probability of positron annihilating with high momentum core electrons, the annihilation characteristics of positrons at defects will be different from the delocalized bulk state: the positron lifetime will become longer and the Doppler broadening of annihilation radiation will be narrower. Therefore, by measuring such positron annihilation characteristics, we can get detailed information about defects. Up to now, several works have been conducted on the study of defects in ZnO by PAS.<sup>25-33</sup>

Except for defects in the as-grown state, they can also be introduced by many other ways, such as irradiation or plastic deformation. High energy electron irradiation is one of the effective ways to introduce simple and number controllable defects. This will help us study defects and their thermal

TABLE I. ZnO samples and the positron lifetime data measured before and after annealing or electron irradiation with dose of  $5.5 \times 10^{18} \text{ cm}^{-2}$ .

ZnO	Treatment	$\tau_1$ (ps)	$\tau_2$ (ps)	$I_2$ (%)	$\tau_{av}$ (ps)
Sample A	As grown	189		0	189
	1000 °C annealed	182		0	182
Sample B	As grown	183		0	183
	1000 °C annealed	183		0	183
	Electron irradiated	152	230	77.3	212
Sample C	As grown	183		0	183
	Electron irradiated	157	231	71.9	210

stability in more detail. On the other hand, study of radiation-induced defects is also important for the space application of ZnO, because these defects play an important role in the degradation of devices used in the space environment. A full understanding of the resistance to radiation is thus necessary before its space application. Nevertheless, the study of radiation effect in ZnO using PAS is still very scarce<sup>25,27,30,31</sup> and far to be comprehensive. In this paper, we studied the vacancy defects introduced by 3 MeV electron irradiation in ZnO single crystals and investigated their thermal recovery process using positron annihilation, Raman scattering, and cathodoluminescence measurements.

## II. EXPERIMENT

ZnO samples are hydrothermal grown single crystals purchased from the Scientific Production Company (SPC Goodwill). They are undoped *n* type with (0001) orientation. Two series of sample are used in this work, which are purchased at different times. The first series (sample A) was annealed from room temperature up to 1000 °C. No electron irradiation experiment was conducted for these samples. The second series is further divided into two categories according to different treatments. One sample (sample B) was annealed at 1000 °C before electron irradiation, and another sample (sample C) was directly irradiated with electrons without preannealing. Annealing was performed in N<sub>2</sub> or O<sub>2</sub> atmosphere for a period of 2 h. Electron irradiation was performed at room temperature using a dynamitron accelerator. The samples were irradiated on Zn face. The incident energy of electrons was 3 MeV and the average fluence rate was  $4.5 \times 10^{13} \text{ cm}^{-2} \text{ s}^{-1}$ . The total electron dose was  $5.5 \times 10^{18} \text{ cm}^{-2}$ . During electron irradiation, samples were cooled by a water cooling system, and the temperature was kept below 70 °C. The irradiated samples were annealed from 100 to 700 °C in nitrogen ambient. Each annealing time was 30 min.

Positron lifetime measurement was performed using a fast-fast coincidence system with time resolution of about 210 ps. Conventional Doppler broadening spectra were measured using a high purity (HP)-Ge detector with energy resolution of about 1.3 keV at 511 keV. The Doppler spectra are characterized by the *S* and *W* parameters, which are defined

as the ratio of the central region ( $511 \pm 0.85 \text{ keV}$ ) and wing region ( $511 \pm 3.4$  to  $511 \pm 6.8 \text{ keV}$ ) to the total area of the 511 keV annihilation peak, respectively. In this work, the *S* and *W* parameters were normalized to the defect-free bulk value. Therefore,  $S > 1$  or  $W < 1$  means existence of vacancy defects. Coincidence Doppler broadening measurements were performed using two HP-Ge detectors. The <sup>22</sup>Na positron source was sandwiched between two pieces of identical sample for measurements. Temperature dependent measurements were carried out by mounting the source-sample sandwich to the cold finger of a He-cycling refrigerator. The temperature range is from 5 to 295 K. The positron source intensity was about 10 μCi for room temperature measurement and about 30 μCi for low temperature measurement, respectively.

CL was measured at room temperature using a modified scanning electron microscope (TOPCON DS-130).<sup>34</sup> A monochromator with grating of 100 lines/mm (Jobin Yvon HR320) and a charge-coupled device were used for the detection of spectra. The electron beam energy was 5 keV and beam current was about 1 nA. The acquisition time for each measurement was 5 s. Micro-Raman-scattering measurements were performed using the Nanofinder spectrometer. The 488.0 nm line of an Ar<sup>+</sup>-ion laser was used for excitation. The incident laser power was ~1 mW and the measurement time for each spectrum was 60 s. All the above measurements were repeated at least one time to ensure reproducibility of the data.

## III. RESULTS AND DISCUSSION

### A. Grown-in defects in ZnO

In this paper, we studied three ZnO samples which have different properties and are subjected to different treatments. The sample treatments and measured positron lifetime data for the three samples are listed in Table I. The positron lifetime spectra are analyzed by PATFIT program.<sup>35</sup> In all the three as-grown samples, decomposition of positron lifetime spectra shows only one lifetime component. In the first sample (sample A), the positron lifetime is about 189 ps, while in samples B and C, the positron has the same lifetime value, i.e., 183 ps. The only one lifetime component does not

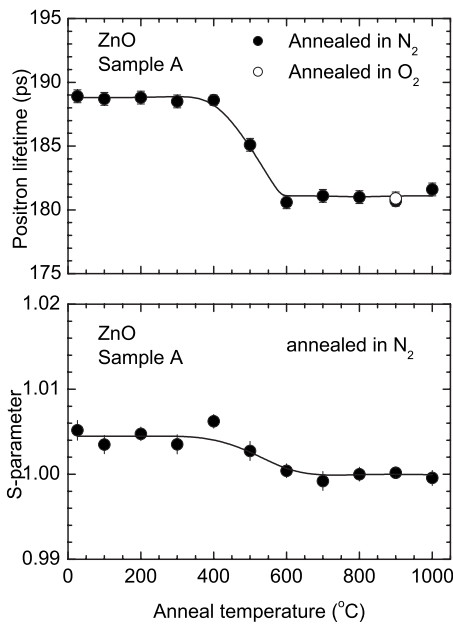


FIG. 1. Average positron lifetime  $\tau_{av}$  and  $S$  parameter as a function of annealing temperature measured for ZnO sample A.

mean that there are no defects that trap positrons. Obviously, a higher positron lifetime in sample A suggests the existence of vacancy defects.

Figure 1 shows the variation of positron lifetime with annealing temperature in sample A. The positron lifetime has no change up to annealing temperature of 400 °C. However, above 400 °C, it begins to decrease, drops to about 181 ps at 600 °C, and then remains nearly constant up to 1000 °C. The Doppler broadening  $S$  parameter shows similar change as shown in Fig. 1. Another as-grown sample A was annealed in O<sub>2</sub> ambient at 900 °C, and the positron lifetime also decreases to about 181 ps. For sample B, after annealing at 1000 °C in N<sub>2</sub>, the positron lifetime shows no change (Table I). These results confirm that sample A contains vacancy-type defects that trap positrons, and they can be removed after annealing above 600 °C. The value of  $182 \pm 1$  ps might be the positron bulk lifetime.

Figure 2 shows the positron lifetime and  $S$  parameter as a function of temperature from 5 to 300 K measured for sample A before and after annealing. For the as-grown sample, the positron lifetime or  $S$  parameter shows notable temperature dependence. The positron lifetime decreases to about 180 ps at  $\sim 5$  K. However, after annealing at 900 °C, such temperature dependence is greatly reduced, and the positron lifetime shows only about 2 ps decrease, which might be attributed to lattice thermal expansion effect.

The temperature behavior exhibited in as-grown sample A is generally explained by the competitive positron trapping by negative ions at low temperatures.<sup>36</sup> As the positron binding energy of these negative ions is rather small ( $< 100$  meV), they are called shallow positron traps. The positron annihilation characteristics at these centers are very close to the bulk state. With increasing temperature, positrons are detrapped from these centers and shift to vacancy-type defects. Therefore, the positron lifetime or  $S$  parameter increases.

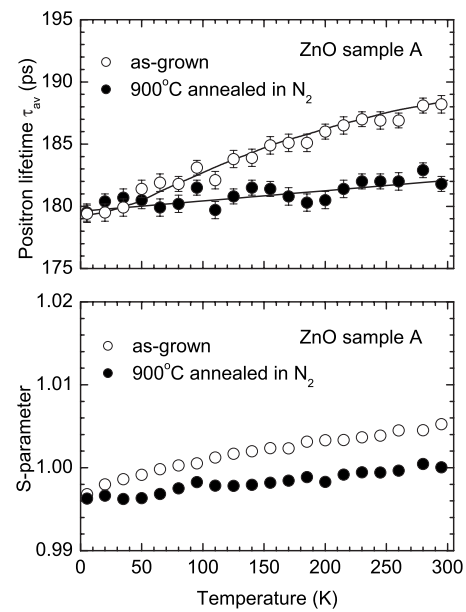


FIG. 2. Temperature dependences of the average positron lifetime and  $S$  parameter in ZnO sample A measured before and after annealing at 900 °C.

However, another possible reason for such temperature behavior cannot be excluded, i.e., the change of the positron trapping rate with temperature. By supposing that the thermally activated trapping of positrons is analog to the capture of free carriers through multiphonon emission,<sup>37–39</sup> the positron trapping rate will increase with temperature. Therefore, detailed fundamental studies are still needed to find out the underlying mechanism for such temperature behavior.

In any case, the temperature dependence of positron annihilation parameter (lifetime or  $S$  parameter) appears only in the existence of positron trapping by vacancy defects. Without vacancy trapping centers to compete with, the shallow traps cannot be observed. Therefore, the disappearance of temperature dependence after annealing sample A at 900 °C confirms that all the vacancies are annealed out, and positron bulk lifetime in the hydrothermally grown ZnO sample is about  $182 \pm 1$  ps.

The origin of the positron trapping centers in as-grown sample A might be  $V_{Zn}$ -related defects, as  $V_O$  is not an effective positron trap.<sup>30</sup> In hydrothermally grown ZnO crystals, hydrogen is easily incorporated into the sample during growth. These hydrogen atoms may fill the zinc vacancy site and form complexes as suggested by Lavrov *et al.*<sup>40</sup> The positron lifetime in  $V_{Zn}$  will then be reduced due to the occupation of hydrogen and become closer to the positron bulk lifetime in ZnO. This may explain why the defect lifetime component cannot be resolved from the lifetime spectrum. However, the hydrogen will become unstable at high temperatures and desorption of hydrogen occurs when annealing the ZnO sample at around 500–700 °C.<sup>41,42</sup> This will restore the open space of  $V_{Zn}$  and cause an increase of positron lifetime. However, in our ZnO sample, we observed a decrease of positron lifetime after annealing. This reveals that the defects are not hydrogen-vacancy complexes. The concentration of  $V_{Zn}$  may be too low, so that the defect related positron lifetime cannot be resolved.

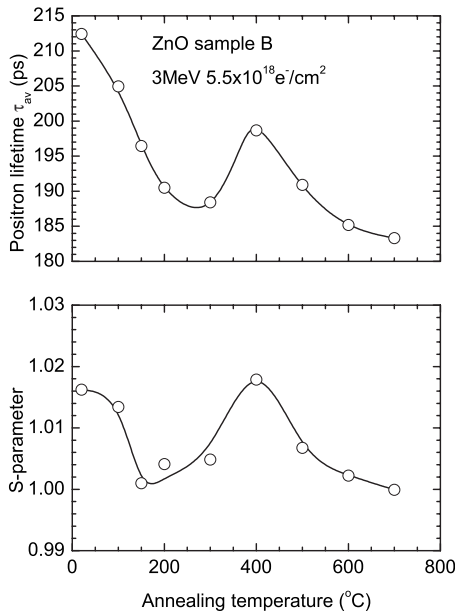


FIG. 3. Average positron lifetime and  $S$  parameter as a function of annealing temperature in electron-irradiated ZnO (sample B) with dose of  $5.5 \times 10^{18} \text{ cm}^{-2}$ . The annealing time was 30 min.

### B. Electron-irradiation-induced defects and their thermal evolution

Samples B and C have the same positron lifetime of 183 ps in the as-grown state, which is close to the lifetime value of annealed sample A. The annealing of sample B does not cause any change of positron lifetime (Table I). So, we believe that no or very few vacancy defects exist in these two samples which trap positrons. After electron irradiation with a dose of  $5.5 \times 10^{18} \text{ cm}^{-2}$ , the average positron lifetime increases up to about 212 and 210 ps for samples B and C, respectively. The Doppler broadening  $S$  parameter also increases to about 1.016 and 1.012 (Figs. 3 and 4). This means that vacancy-type defects are introduced by electron irradiation. After irradiation, we can decompose the lifetime spectra into two components, and  $\tau_2$  corresponds to positron lifetime at vacancy defects, which is about 230 ps. This value is in agreement with that reported by Tuomisto *et al.*<sup>30</sup> As the ratio of  $\tau_2/\tau_b$  is around 1.26, this corresponds to positron lifetime at monovacancies.

In ZnO, both  $V_{\text{Zn}}$  and  $V_{\text{O}}$  may be introduced after electron irradiation. However, as described above,  $V_{\text{O}}$  might be less possible to be positron trapping centers. Therefore, the vacancies observed by positrons in the electron-irradiated ZnO are also  $V_{\text{Zn}}$ -related defects. The positron trapping rate  $\kappa$  was calculated according to the two state trapping model:  $\kappa = (\tau_{av} - \tau_b) / (\tau_2 - \tau_{av}) / \tau_b$ . According to the trapping model, there is a quantitative relationship between trapping rate and defect concentration:  $\kappa = \mu C_d$ , where  $\mu$  is the specific positron trapping rate. Taking the value of  $\mu = 3 \times 10^{15} \text{ s}^{-1}$  for  $V_{\text{Zn}}$  as suggested by Tuomisto *et al.*,<sup>30</sup> the electron-irradiation-induced vacancy concentration is about  $2.6 \times 10^{17}$  and  $2.1 \times 10^{17} \text{ cm}^{-3}$  for samples B and C, respectively. This corresponds to a defect introduction rate of  $0.04\text{--}0.05 \text{ cm}^{-1}$ , in agreement with the result obtained by Tuomisto *et al.*<sup>31</sup>

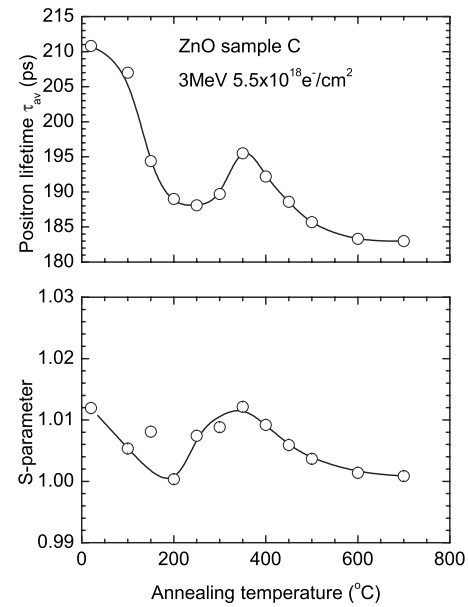


FIG. 4. Average positron lifetime and  $S$  parameter as a function of annealing temperature in electron-irradiated ZnO (sample C) with dose of  $5.5 \times 10^{18} \text{ cm}^{-2}$ . The annealing time was 30 min.

The two electron-irradiated samples are subjected to annealing up to 700 °C. The change of average positron lifetime and  $S$  parameter after annealing is shown in Figs. 3 and 4. The annealing behavior is nearly the same for these two samples. A fast decrease of both positron lifetime and  $S$  parameter is seen below 200 °C. After that, both of them begin to increase and reach a maximum value at 350–400 °C. Above 400 °C, the positron lifetime and  $S$  parameter decrease again and approach the bulk value at 700 °C.

The decrease of positron lifetime and  $S$  parameter below 200 °C is attributed to the recombination of  $V_{\text{Zn}}\text{-Zn}_i$  close Frenkel pairs. Tomiyama *et al.*<sup>25</sup> observed similar annealing stage for the 28 MeV electron-irradiated ZnO, which was around 150–200 °C. This was in agreement with our result. They attributed this annealing stage to the recovery of irradiation induced oxygen vacancies, but that is not likely, as oxygen vacancies cannot be detected by positrons. On the other hand, oxygen vacancy may remain stable up to 400 °C.<sup>43</sup> The same annealing stage at 50–150 °C was also observed by Brunner *et al.*<sup>27</sup> in the 2 MeV electron-irradiated ZnO, and it was attributed to the annealing of Zn monovacancies.

As for the abnormal increase of the positron lifetime after annealing at 350–400 °C, there are two possible reasons. One reason might be the shift of the Fermi level to a higher value after annealing of the irradiated sample; therefore, the vacancy defects become more negatively charged, which leads to an increase of positron trapping rate. In order to check such possibility, we measured the electrical conductivity of the irradiated sample after annealing by Hall effect. The results are listed in Table II. The resistivity of the sample before electron irradiation is about 250  $\Omega \text{ cm}$ , but it becomes semi-insulating after irradiation. Even after 400 °C annealing, it still keeps high resistivity. Only after annealing at 600 °C, the resistivity recovers to that of the unirradiated

TABLE II. Resistivity  $\rho$  in the ZnO sample (sample B) before and after electron irradiation and annealing determined from the Hall measurements.

Sample treatment	$\rho$ ( $\Omega$ cm)	Type
Unirradiated	247	<i>n</i>
As irradiated		SI
200 °C annealed		SI
400 °C annealed	$6.7 \times 10^4$	SI
600 °C annealed	275	<i>n</i>

state, i.e., 275  $\Omega$  cm. This means that the Fermi level does not move after annealing up to 400 °C, which is pinned at around the midgap position. Therefore, the increase of positron lifetime is not due to the shift of the Fermi level.

By excluding the possibility of the Fermi level movement, the second reason for the increase of positron lifetime after annealing at 400 °C would be the introduction of some additional open volume defects. These defects might be formed due to defect reaction at high temperatures. Nevertheless, we do not observe much change of the defect lifetime  $\tau_2$  after formation of the secondary defects. However, this does not mean that the secondary defect is still  $V_{Zn}$ . After annealing at 400 °C, the defect concentration is largely reduced, so the decomposition of positron lifetime spectrum is not reliable. Even if the positron lifetime for the secondary defect is different from that of  $V_{Zn}$ , we cannot get its accurate value. On the other hand, the secondary defects might be  $V_{Zn}$ -impurity complexes, which have positron lifetime close to that of  $V_{Zn}$ . Brunner *et al.*<sup>27</sup> also observed an increase of positron lifetime and *S* parameter after annealing the electron irradiated ZnO at around 300 °C, and they believe that it is due to agglomeration of nonannealed defects to more stable complexes, such as  $V_{Zn}$ -donor complex.<sup>27</sup>

A detailed analysis of the correlation between *S* and *W* parameters from the Doppler broadening measurements gives us more complementary information about the defect evolution that occurred during annealing. Figure 5 shows the *S*-*W* plot obtained from the annealing measurements for electron-irradiated samples B and C. In the annealing process, the *S*-*W* data are concentrated on two different lines, which correspond to two different types of defects, i.e., the electron-irradiation-induced  $V_{Zn}$  (defect 1) and the annealing produced secondary defects (defect 2). It is interesting to note that in samples B and C, the *S*-*W* data are concentrated on the two same lines. Therefore, this confirms that annealing at 350–400 °C produces additional vacancy defects which are different from  $V_{Zn}$  introduced by irradiation.

To further identify the difference between the irradiation-induced  $V_{Zn}$  and the thermally generated secondary defects, we also conducted the coincidence Doppler broadening measurements for electron-irradiated sample C. The peak to background ratio of the measured spectrum is higher than  $10^5$ . The ratio curves are shown in Fig. 6. The reference sample is unirradiated sample C. It is clear to see that the ratio curves at the low momentum region for the asirradiated and 400 °C annealed sample are nearly the same; thus, the *S*

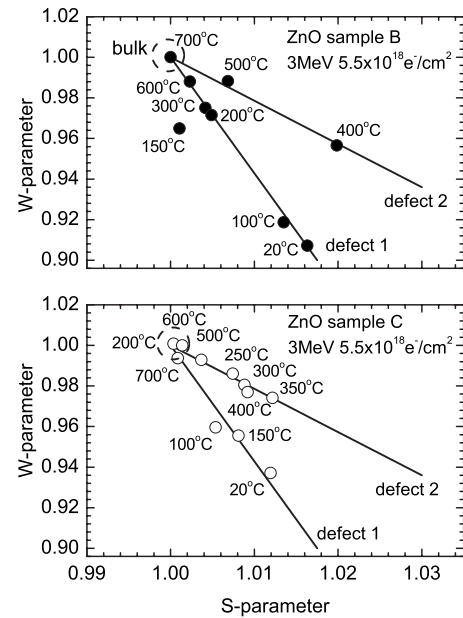


FIG. 5. *S*-*W* plot from the Doppler broadening measurement in electron-irradiated ZnO samples B and C.

parameter has nearly the same value as seen in Figs. 3 and 4. However, the high momentum region shows much difference. After 400 °C annealing, the center of the valley in the high momentum region shifted from  $\sim 20 \times 10^{-3} m_0c$  to lower than  $10 \times 10^{-3} m_0c$ , and becomes much smaller. This coincides with the higher *W* parameter after annealing, indicating different defect species.

After annealing above 400 °C, the positron lifetime and *S* parameter show a decrease again. It can be inferred that the remaining  $V_{Zn}$  are removed in this stage through migration into sinks. The secondary defects created at around 400 °C also become unstable and are annealed out at 700 °C as both positron lifetime and *S* parameter decrease to the bulk value.

We measured temperature dependence of the positron lifetime and Doppler broadening spectra for the irradiated sample B before and after annealing. The result is shown in Fig. 7. For the asirradiated sample, the average positron lifetime first remains nearly constant below 100 K, and then

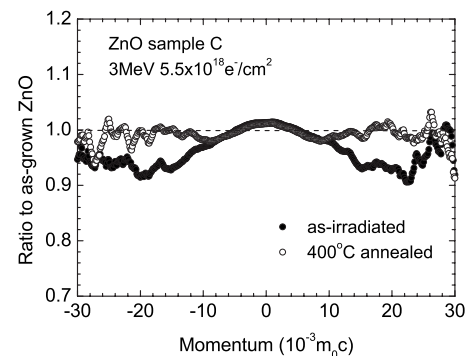


FIG. 6. Ratio curve of the Doppler broadening spectrum of electron-irradiated ZnO sample C before and after annealing measured using a coincidence Doppler broadening spectrometer. The reference sample is the unirradiated ZnO sample C.

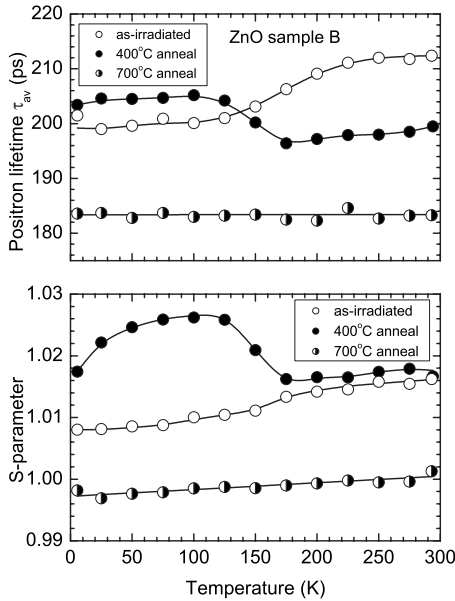


FIG. 7. Temperature dependences of the average positron lifetime and  $S$  parameter in electron-irradiated ZnO (sample B) before and after annealing.

starts to increase with temperature. Afterward, it tends to be saturated above 250 K. The  $S$  parameter shows similar temperature behavior. These results suggest that the positron trapping by vacancy defects is temperature dependent, possibly due to the trapping by shallow positron traps at low temperatures. The negatively charged antisites or interstitials like  $O_{Zn}$  and  $O_i$  which are produced by irradiation might act as such shallow traps.

After annealing the irradiated sample at 400 °C, where we observe the production of secondary defects, the temperature dependence of positron lifetime and  $S$  parameter is, however, quite different from that of the asirradiated sample. There is an increase of positron lifetime at around 100–180 K when the temperature decreases. The  $S$  parameter also shows similar change at this temperature range. This means that positron trapping by the secondary defects is enhanced below 180 K, or the secondary defects undergo a charge state transition and become more negatively charged at lower temperatures, which causes an increase of positron lifetime. Below 100 K, the negative ions begin to compete with deep traps, and positron lifetime shows a decrease. We repeat the same temperature dependence measurement for the irradiated sample C after annealing at 400 °C, and observed quite similar result, which is shown in Fig. 8. Therefore, from the temperature dependence of the positron annihilation parameters, it suggests again that the defects created after annealing at 400 °C are different from the irradiation-induced  $V_{Zn}$ .

After annealing the irradiated sample at 700 °C, both positron lifetime and  $S$  parameter show very slight increase or nearly no change with temperature (Fig. 7). This confirms that all the vacancy defects have been removed by annealing.

At present, we cannot clarify the species of the secondary defects. In order to understand more deeply the thermal evolution of the electron-irradiation-induced defects, we also

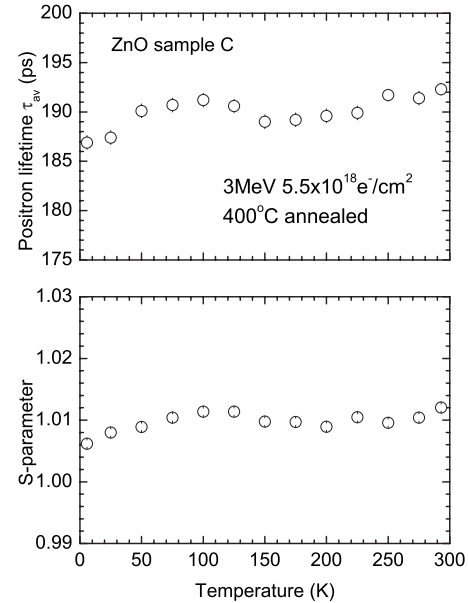


FIG. 8. Temperature dependences of the average positron lifetime and  $S$  parameter in electron-irradiated ZnO (sample C) before and after annealing.

performed Raman scattering measurements. Figure 9 shows the Raman spectra for the electron-irradiated ZnO (sample B) before and after annealing. The detailed assignment of the Raman peaks in ZnO can be found in many literature<sup>44,45</sup> and also our previous paper.<sup>42</sup> The primary peak at 437  $cm^{-1}$  is the high frequency  $E_2$  phonon mode, which represents the wurtzite structure of ZnO. The peak at 331  $cm^{-1}$  is due to the second order phonon. After electron irradiation, a broad peak at 575  $cm^{-1}$  appears. This broad peak is obviously induced

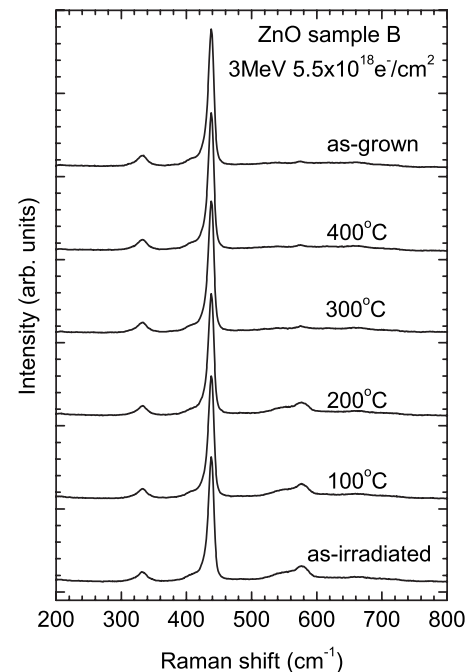


FIG. 9. Annealing effect on the Raman spectra measured for the electron-irradiated ZnO (sample B).

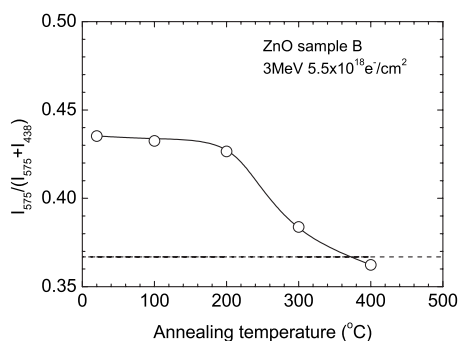
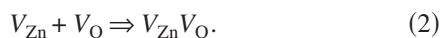


FIG. 10. Ratio of the integrated  $575\text{ cm}^{-1}$  peak intensity to the sum of the  $437$  and  $575\text{ cm}^{-1}$  peaks as a function of annealing temperature for the electron-irradiated ZnO sample B.

by the defects produced by electron irradiation because of the relaxation of the Raman selection rules.<sup>44</sup>

After annealing up to  $200\text{ }^\circ\text{C}$ , the broad peak at  $575\text{ cm}^{-1}$  shows very small decrease. This indicates that the defects are stable at least up to  $200\text{ }^\circ\text{C}$ . After  $300\text{ }^\circ\text{C}$  annealing, such peak becomes much weaker, and at  $400\text{ }^\circ\text{C}$ , it decreases to the same level as that of the as-grown sample. Figure 10 shows the ratio of the integrated intensity of the broad peak at  $575\text{ cm}^{-1}$  to the sum of the  $575$  and  $437\text{ cm}^{-1}$  peaks. It is clear that the broad peak intensity begins to decrease at  $300\text{ }^\circ\text{C}$  and reaches the value of the as-grown sample at  $400\text{ }^\circ\text{C}$ . As the positron annihilation measurements show that most of the  $V_{\text{Zn}}$ -related defects disappear at temperatures below  $200\text{ }^\circ\text{C}$ , the broad Raman peak is apparently not related to  $V_{\text{Zn}}$ . This means that the defect is invisible to positrons. The broad peak at  $575\text{ cm}^{-1}$  has been suggested to be related to oxygen vacancies or zinc interstitials by many researchers,<sup>46–48</sup> as they found that such broad peak will be enhanced in an oxygen deficient condition.

The Raman measurements show that the  $575\text{ cm}^{-1}$  peak begins to recover above  $200\text{ }^\circ\text{C}$  and disappears at around  $400\text{ }^\circ\text{C}$ . This is in good agreement with the result that the oxygen vacancies are annealed at  $400\text{ }^\circ\text{C}$  in electron-irradiated ZnO measured by Vlasenko and Watkins.<sup>43</sup> Therefore, the possible candidate for this defect would be oxygen vacancy. The annealing behavior shows that  $V_{\text{O}}$  becomes mobile at  $200\text{--}400\text{ }^\circ\text{C}$ , which coincides with the temperature for the production of secondary defects. Thus, we may assume that while some of the  $V_{\text{O}}$  disappear through recombination with their interstitials or migration into sinks, many of them might also take part in the following defect reactions:



Therefore, formation of  $V_{\text{Zn}}\text{--ZnO}$  complexes or agglomeration of  $V_{\text{Zn}}$  into divacancies is the possible candidate for the secondary defects, which result in the increase of positron lifetime and  $S$  parameter after annealing at  $350\text{--}400\text{ }^\circ\text{C}$ . However, further experiments and theoretical calculations are still needed to confirm such speculation.

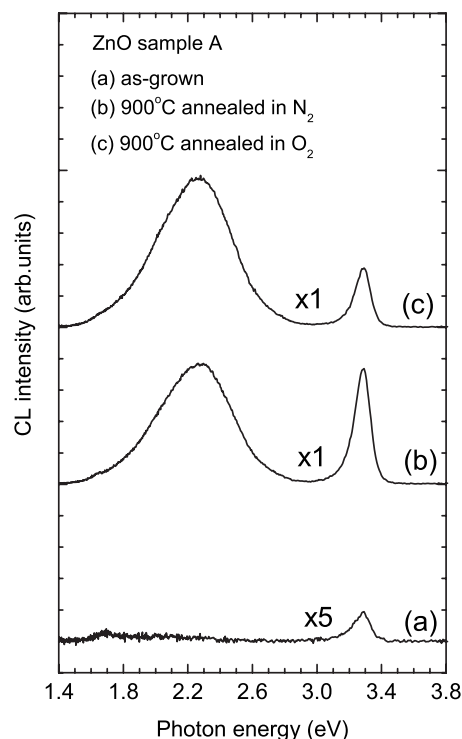


FIG. 11. Annealing effect on the cathodoluminescence spectra measured for the as-grown ZnO (sample A).

### C. Correlation between defects and luminescence centers

The cathodoluminescence spectra measured for sample A in the as-grown state and after annealing at  $900\text{ }^\circ\text{C}$  are shown in Fig. 11. In the as-grown sample, there is only one weak peak at about  $3.3\text{ eV}$ . This is the ultraviolet (UV) emission due to the recombination of free excitons. The rather weak UV emission indicates that a large number of nonradiative recombination centers exist in the as-grown ZnO sample. These nonradiative recombination centers are most probably grown-in defects, which suppress both UV and deep level (visible) emission.

After annealing sample A in  $\text{N}_2$  at  $900\text{ }^\circ\text{C}$ , the UV emission peak is strongly enhanced. The peak height increases by almost 20 times. The visible emission also appears, which is located at around  $2.3\text{ eV}$ . This emission obviously originates from the deep level defects. When sample A is annealed in  $\text{O}_2$  ambient, both UV and visible emission also show increase. However, the UV emission is much lower compared with the  $\text{N}_2$  annealed one, while the visible emission is stronger. This indicates that annealing atmosphere has some influence on the formation of deep level defects.

Figure 12 presents the CL spectra measured for ZnO sample C before and after electron irradiation and annealing. For the as-grown sample, the UV and visible emission intensities are higher than those of sample A. After irradiation, the UV emission peak is weakened, while the deep level emission shows an increase. Annealing of the irradiated sample up to  $300\text{ }^\circ\text{C}$  causes a gradual recovery of the light emission. However, after annealing at  $400\text{ }^\circ\text{C}$ , the visible emission at  $\sim 2.3\text{ eV}$  shows abrupt increase. This reveals again that defect reaction really happened during annealing, which results

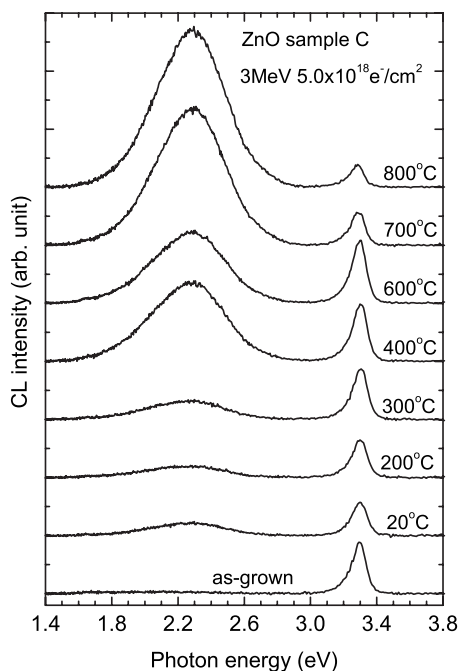


FIG. 12. Annealing effect on the cathodoluminescence spectra measured for the electron-irradiated ZnO (sample C) with dose of  $5.0 \times 10^{18} \text{ cm}^{-2}$ .

in the formation of secondary vacancy defects at around 400 °C. The visible emission becomes even stronger after annealing at 700–800 °C, and thereby the UV emission becomes much weaker.

Combining the positron annihilation and cathodoluminescence results, we can find that there is no correlation between the deep level emission and zinc vacancy. In the as-grown sample A, the deep level emission is too weak to be seen in the spectrum. It becomes much stronger after annealing at 900 °C. Contrarily, the positron measurements show the reduction of  $V_{\text{Zn}}$  after annealing. In the as-grown ZnO sample C, which has nearly no positron trapping by  $V_{\text{Zn}}$ , however, the deep level emission is stronger than that of sample A. Furthermore, in the electron-irradiated ZnO (for example, sample C), the annealing process of deep level emission is also different from that of  $V_{\text{Zn}}$ . Thus,  $V_{\text{Zn}}$  is not related to the deep level emission at 2.3 eV in ZnO. This defect would

rather be responsible for the nonradiative recombination centers. When these defects exist in ZnO, both the UV and visible emission will be suppressed. Thus, we can explain the weak CL signal in as-grown sample A, the enhancement after annealing, and also the stronger CL signal in as-grown sample C. In the electron-irradiated sample C, though the irradiation introduces nonradiative recombination centers, deep level emission centers are also introduced; thus, the UV emission is weakened, but the visible emission is enhanced.

As for the candidates for the deep level emission centers, our results may provide some suggestions. When the as-grown ZnO sample was annealed in  $\text{O}_2$  ambient, the formation of deep level centers is favored. This suggests that the deep level defects might be associated with oxygen, for example, the antisite  $\text{O}_{\text{Zn}}$  as suggested by Lin *et al.*,<sup>20</sup> or interstitial  $\text{O}_i$ . These defects are easier to be formed during annealing in  $\text{O}_2$  atmosphere. Tuomisto *et al.* also found that the negative-ion-type defects such as  $\text{O}_i$  or  $\text{O}_{\text{Zn}}$  had ionization levels close to 2.3 eV, and thus are possibly involved in the green luminescence.<sup>31</sup>

#### IV. CONCLUSION

Defects in the as-grown and electron-irradiated ZnO crystals were studied by positron annihilation spectroscopy. The grown-in defects in ZnO seen by positron are  $V_{\text{Zn}}$ -related defects and can be removed by annealing above 600 °C. Electron irradiation also introduces  $V_{\text{Zn}}$  in ZnO. Annealing below 200 °C causes partial recovery of these vacancies. However, after annealing at around 400 °C, additional vacancy defects are produced. The *S-W* correlation and coincidence Doppler broadening study reveals that these two vacancy defects are not the same category. All the vacancy defects are annealed out at around 700 °C. The zinc vacancy in ZnO is found to be not related to the deep level emission at 2.3 eV, but would rather be responsible for the nonradiative recombination centers.

#### ACKNOWLEDGMENTS

This work was partly supported by the Program for New Century Excellent Talents in University and the National Natural Science Foundation of China under Grant Nos. 10475062 and 10075037.

\*chenzq@whu.edu.cn

<sup>1</sup>D. C. Look, D. C. Reynolds, J. R. Sizelove, R. L. Jones, C. W. Litton, G. Cantwell, and W. C. Harsch, *Solid State Commun.* **105**, 399 (1998).

<sup>2</sup>S. J. Pearton, D. P. Norton, K. Ip, Y. W. Heo, and T. Steiner, *Prog. Mater. Sci.* **90**, 293 (2005).

<sup>3</sup>U. Ozgur, Ya I. Alivov, C. Liu, A. Teke, M. A. Reshchikov, S. Dogan, V. Avrutin, S.-J. Cho, and H. Morkoc, *J. Appl. Phys.* **98**, 041301 (2005).

<sup>4</sup>D. C. Look, J. W. Hemsky, and J. R. Sizelove, *Phys. Rev. Lett.* **82**, 2552 (1999).

<sup>5</sup>D. C. Look, G. C. Farlow, Pakpoom Reunchan, Sukit Limpijum-nong, S. B. Zhang, and K. Nordlund, *Phys. Rev. Lett.* **95**, 225502 (2005).

<sup>6</sup>Eun-Cheol Lee, Y.-S. Kim, Y.-G. Jin, and K. J. Chang, *Phys. Rev. B* **64**, 085120 (2001).

<sup>7</sup>A. F. Kohan, G. Ceder, D. Morgan, and Chris G. Van de Walle, *Phys. Rev. B* **61**, 15019 (2000).

<sup>8</sup>F. Oba, S. R. Nishitani, S. Isotani, H. Adachi, and I. Tanaka, *J. Appl. Phys.* **90**, 824 (2001).

<sup>9</sup>S. B. Zhang, S.-H. Wei, and Alex Zunger, *Phys. Rev. B* **63**, 075205 (2001).

- <sup>10</sup>P. H. Kasai, Phys. Rev. **130**, 989 (1963).
- <sup>11</sup>N. Ohashi, T. Nakata, T. Sekiguchi, H. Hosono, M. Mizuguchi, T. Tsurumi, J. Tanaka, and H. Haneda, Jpn. J. Appl. Phys., Part 2 **38**, L113 (1999).
- <sup>12</sup>K. Vanheusden, C. H. Seager, W. L. Warren, D. R. Tallant, and J. A. Voigt, Appl. Phys. Lett. **68**, 403 (1996).
- <sup>13</sup>X. L. Wu, G. G. Siu, C. L. Fu, and H. C. Ong, Appl. Phys. Lett. **78**, 2285 (2001).
- <sup>14</sup>F. K. Shan, G. X. Liu, W. J. Lee, G. H. Lee, I. S. Kim, and B. C. Shin, Appl. Phys. Lett. **86**, 221910 (2005).
- <sup>15</sup>T. Moe Borseth, B. G. Svensson, A. Yu. Kuznetsov, P. Klason, Q. X. Zhao, and M. Willander, Appl. Phys. Lett. **89**, 262112 (2006).
- <sup>16</sup>D. C. Reynolds, D. C. Look, B. Jogai, J. E. Van Nostrand, R. Jones, and J. Jenny, Solid State Commun. **106**, 701 (1998).
- <sup>17</sup>Q. X. Zhao, P. Klason, M. Willander, H. M. Zhong, W. Lu, and J. H. Yang, Appl. Phys. Lett. **87**, 211912 (2005).
- <sup>18</sup>M. Liu, A. H. Kitai, and P. Mascher, J. Lumin. **54**, 35 (1992).
- <sup>19</sup>S.-H. Jeong, B.-S. Kim, and B.-T. Lee, Appl. Phys. Lett. **82**, 2625 (2003).
- <sup>20</sup>B. Lin, Z. Fu, and Y. Jia, Appl. Phys. Lett. **79**, 943 (2001).
- <sup>21</sup>T.-B. Hur, G. S. Jeon, Y.-H. Hwang, and H.-K. Kim, J. Appl. Phys. **94**, 5787 (2003).
- <sup>22</sup>N. Y. Garces, L. Wang, L. Bai, N. C. Giles, L. E. Halliburton, and G. Cantwell, Appl. Phys. Lett. **81**, 622 (2002).
- <sup>23</sup>J. C. Simpson and J. F. Cordaro, J. Appl. Phys. **63**, 1781 (1988).
- <sup>24</sup>R. Krause-Rehberg and H. S. Leipner, *Positron Annihilation in Semiconductors, Defect Studies*, Springer Series in Solid-State Sciences Vol. 127 (Springer, Berlin, 1999).
- <sup>25</sup>N. Tomiyama, M. Takenaka, and E. Kuramoto, Mater. Sci. Forum **105-110**, 1281 (1992).
- <sup>26</sup>R. M. de la Cruz, R. Pareja, R. González, L. A. Boatner, and Y. Chen, Phys. Rev. B **45**, 6581 (1992).
- <sup>27</sup>S. Brunner, W. Puff, A. G. Balogh, and P. Mascher, Mater. Sci. Forum **363-365**, 141 (2001).
- <sup>28</sup>A. Uedono, T. Koida, A. Tsukazaki, M. Kawasaki, Z. Q. Chen, S. F. Chichibu, and H. Koinuma, J. Appl. Phys. **93**, 2481 (2003).
- <sup>29</sup>Z. Q. Chen, S. Yamamoto, M. Maekawa, A. Kawasuso, X. L. Yuan, and T. Sekiguchi, J. Appl. Phys. **94**, 4807 (2003).
- <sup>30</sup>F. Tuomisto, V. Ranki, K. Saarinen, and D. C. Look, Phys. Rev. Lett. **91**, 205502 (2003).
- <sup>31</sup>F. Tuomisto, K. Saarinen, D. C. Look, and G. C. Farlow, Phys. Rev. B **72**, 085206 (2005).
- <sup>32</sup>S. Dutta, S. Chattopadhyay, D. Jana, A. Banerjee, S. Manik, S. K. Pradhan, Manas Sutradhar, and A. Sarkar, J. Appl. Phys. **100**, 114328 (2006).
- <sup>33</sup>G. Brauer, W. Anwand, W. Skorupa, J. Kuriplach, O. Melikhova, C. Moisson, H. von Wenckstern, H. Schmidt, M. Lorenz, and M. Grundmann, Phys. Rev. B **74**, 045208 (2006).
- <sup>34</sup>T. Sekiguchi and K. Sumino, Rev. Sci. Instrum. **66**, 4277 (1995).
- <sup>35</sup>P. Kirkegaard, N. J. Pederson, and M. Eldrup, Risø National Laboratory, DK-4000 Roskilde, Denmark, 1989.
- <sup>36</sup>K. Saarinen, P. Hautojärvi, A. Vehanen, R. Krause, and G. Dlubek, Phys. Rev. B **39**, 5287 (1989).
- <sup>37</sup>C. H. Henry and D. V. Lang, Phys. Rev. B **15**, 989 (1977).
- <sup>38</sup>H. Sumi, Phys. Rev. B **27**, 2374 (1983).
- <sup>39</sup>P. Mascher, S. Dannefaer, D. Kerr, and W. Puff, in *Defect Control in Semiconductors*, edited by K. Sumino (Elsevier Science, New York/North Holland, Amsterdam 1990), p. 777.
- <sup>40</sup>E. V. Lavrov, J. Weber, F. Bornert, Chris G. Van de Walle, and R. Helbig, Phys. Rev. B **66**, 165205 (2002).
- <sup>41</sup>K. Ip, M. E. Overberg, Y. W. Heo, D. P. Norton, S. J. Pearton, S. O. Kucheyev, C. Jagadish, J. S. Williams, R. G. Wilson, and J. M. Zavada, Appl. Phys. Lett. **81**, 3996 (2002).
- <sup>42</sup>Z. Q. Chen, A. Kawasuso, Y. Xu, H. Naramoto, X. L. Yuan, T. Sekiguchi, R. Suzuki, and T. Ohdaira, Phys. Rev. B **71**, 115213 (2005).
- <sup>43</sup>L. S. Vlasenko and G. D. Watkins, Phys. Rev. B **71**, 125210 (2005).
- <sup>44</sup>T. C. Damen, S. P. S. Porto, and B. Tell, Phys. Rev. **142**, 570 (1966).
- <sup>45</sup>J. M. Calleja and M. Cardona, Phys. Rev. B **16**, 3753 (1977).
- <sup>46</sup>C. J. Youn, T. S. Jeong, M. S. Han, and J. H. Kim, J. Cryst. Growth **261**, 526 (2004).
- <sup>47</sup>J. N. Zeng, J. K. Low, Z. M. Ren, T. Liew, and Y. F. Lu, Appl. Surf. Sci. **197**, 362 (2002).
- <sup>48</sup>S.-H. Jeong, J.-K. Kim, and B.-T. Lee, J. Phys. D **36**, 2017 (2003).